Pakistan Veterinary Journal

ISSN: 0253-8318 (PRINT), 2074-7764 (ONLINE)
DOI: 10.29261/pakvetj/2025.333

RESEARCH ARTICLE

Multifunctional Biogenic Selenium Nanoparticles from *Citrus sinensis* peel: *In Vivo* Antioxidant, Antiviral, Antibacterial, Anticancer and Neuroprotective Assessment in Rat Model

Amani Osman Shakak[1,2], Karima Bel Hadj Salah[1,3], Mada F. Ashkan[1], Safia M.A. Bahshwan[1], Abeer Mogadem[4], Salwa Aljohani[4], Maha A. Aljumaa[5], Ebtihaj O. Alnasri[6], Alanood A. Alfaleh[6], Marzough Aziz Albalawi[7], Amira K. Hajri[7], Fawzyah Abdullah Al-Ghamdi[8], Zahrah R. Alrayes[9] and Imen Zghab*[10]

[1]Biological Sciences Department, College of Science & Arts, King Abdulaziz University, Rabigh, 21911, Saudi Arabia; [2]University of Shendi, Faculty of Medical Laboratory Sciences, PO Box 142, Shendi, Sudan; [3]Laboratory of Transmissible Diseases and Biologically Active Substances, Faculty of Pharmacy, University of Monastir; Monastir 5019; Tunisia; [4]Department of Chemistry, College of Science, Taibah University, Madinah, Saudi Arabia;[5]Department of Biology, College of Science, Princess Nourah bint Abdulrahman University, P.O. Box 84428, Riyadh 11671, Saudi Arabia; [6]Food and Nutrition Department, Faculty of Human Sciences and Design, King Abdulaziz University, Jeddah, Saudi Arabia; [7]Department of Chemistry, Alwajh College, University of Tabuk, Tabuk 71491, Saudi Arabia; [8]Department of Biological Science, College of Science, University of Jeddah, Jeddah, Saudi Arabia, P.O. Box 80327, Jeddah 21589, Saudi Arabia; [9]Department of Biology, College of Science, Jouf University, 72341 Sakaka, Al-Jouf, Saudi Arabia; [10]Department of Physical Sciences, Chemistry Division, College of Science, Jazan University, P.O. Box. 114, Jazan 45142, Saudi Arabia
*Corresponding author: izghab@jazanu.edu.sa

ARTICLE HISTORY (25-1022)

Received: October 25, 2025
Revised: December 17, 2025
Accepted: December 21, 2025
Published online: December 24, 2025

Key words:
Apoptosis
Biogenic selenium nanoparticles
Green synthesis
Multimodal therapy
Neuroprotection
Rat model.

ABSTRACT

The development of innovative, multi-targeted therapeutic agents from sustainable sources is essential in veterinary and biomedical sciences. Green synthesis improves the biocompatibility and utility of selenium nanoparticles (SeNPs). This research synthesized selenium nanoparticles using a polyphenolic-rich *Citrus sinensis* peel extract (Cs-SeNPs) and conducted a comprehensive assessment of their therapeutic efficacy across four principal disease models in Wistar rats. Cs-SeNPs were synthesized via green reduction using Citrus peel extract, yielding spherical particles 25nm in diameter with a negative zeta potential of -22mV. Selenium nanoparticles showed low cytotoxicity (CC_{50} >150µg/mL) in TZM-bl and RAW 264.7 cells. They exhibited significant antiviral activity against HIV-1 (IC_{50} = 58.7µg/mL) and the murine norovirus surrogate MNV-1 (IC_{50} = 41.2µg/mL). Therapeutic efficacy was evaluated in 250 rats across models of CCl_4-induced oxidative stress, *Staphylococcus aureus* and *Escherichia coli*-infected wounds, DMH-induced colon cancer, and ICV-STZ-induced Alzheimer's disease. Cs-SeNPs significantly ($P<0.001$) restored endogenous antioxidant status and reduced lipid peroxidation by 75%. In the wound model, topical Cs-SeNPs achieved 99% wound closure and a 95% decrease in bacterial load within 14 days. Anticancer activity was robust, reducing tumor burden by 70% and inducing apoptosis, as evidenced by a 5-fold increase in the Bax/Bcl-2 ratio. In the neurodegeneration model, Cs-SeNPs significantly enhanced cognitive performance, reduced AChE activity by 45%, and decreased amyloid-beta plaque load by 60%. In conclusion, biogenic Cs-SeNPs constitute a highly efficient, single therapeutic agent exhibiting robust in vivo antioxidant, antimicrobial, anticancer, and anti-Alzheimer's efficacy.

To Cite This Article: Shakak AO, Salah KBH, Ashkan MF, Bahshwan SMA, Mogadem Ab, Aljohani S, Aljumaa MA, Alnasri EO, Alfaleh AA, Albalawi MA, Hajri AK, Al-Ghamdi FA, Alrayes ZR, and Zghab I, 2025. Multifunctional biogenic selenium nanoparticles from *Citrus sinensis* peel: *in vivo* antioxidant, antiviral, antibacterial, anticancer and neuroprotective assessment in rat model. Pak Vet J. http://dx.doi.org/10.29261/pakvetj/2025.333

INTRODUCTION

In veterinary applications, eco-friendly nanomedicine using green-synthesized nanoparticles has gained notable interest as an effective and sustainable approach to animal health management (Youssef *et al.*, 2024; Kazemi, 2025). These nanoparticles are produced through environmentally friendly methods using natural materials—such as citrus

peels or microbial biomass—as reducing and stabilizing agents, thus avoiding the need for toxic chemicals or energy-intensive processes in animal treatments (Alsulami and El-Saadony, 2023; Reda *et al.,* 2024; Thagfan *et al.,* 2025). This bio-inspired synthesis aligns with the twelve principles of green chemistry, particularly waste prevention and the use of safer solvents, ensuring low toxicity and energy efficiency (Reda *et al.,* 2020; Sheiha *et al.,* 2020; Chin *et al.,* 2024; Saxena *et al.,* 2025). The resulting nanoparticles exhibit unique physicochemical properties—including biocompatibility, high surface area, and tunable size—which make them highly suitable for biomedical applications with reduced side effects relative to chemically synthesized counterparts (Ying *et al.*, 2022; Singaravelu *et al.*, 2025).

Green nanoparticles offer a novel platform for targeted drug delivery, enhanced imaging, antimicrobial treatments, and regenerative therapies (Alsulami and El-Saadony, (2024); Saad *et al.,* 2022; El-Saadony *et al.,* 2024), their small size enables them to penetrate tissues and cellular barriers efficiently, while the bioactive compounds from the natural sources used during synthesis confer additional therapeutic effects, such as antioxidant and anti-inflammatory activities (Zahra *et al.*, 2023). Notably, green-synthesized nanoparticles have demonstrated potential in inhibiting cancer cell proliferation, combating drug-resistant microbial infections, protecting nerve cells, and promoting wound healing (Alvi *et al.*, 2021; Ying *et al.,* 2022; El-Saadony *et al.,* 2025). Furthermore, because they are derived from renewable biological resources and avoid hazardous synthesis conditions, these nanoparticles contribute to the Sustainable Development Goals (SDGs), specifically good health and well-being (SDG 3) and responsible consumption and production (SDG 12). This approach reduces environmental impact, which is critical in addressing global health challenges and minimizing ecological risks (Altammar, 2023).

Citrus peels, a major byproduct of the citrus fruit industry, represent a rich and underutilized source of diverse bioactive compounds with substantial health-promoting potential. These peels contain abundant essential oils, carotenoids, pectins, dietary fiber, and a wide array of polyphenols and flavonoids, including major constituents such as hesperidin, naringin, rutin, and neohesperidin (Maqbool *et al.*, 2023). Remarkably, the concentration of these antioxidants phytochemicals in the peel often surpasses that found in the edible pulp, making citrus peel an invaluable resource for nutraceutical and pharmaceutical applications (Saini *et al.*, 2022; Ogo *et al.*, 2024a).

Despite the growing literature on selenium nanoparticles (SeNPs), a significant gap remains regarding multifunctional nanoparticles explicitly derived from *Citrus sinensis* peel. This study is novel in that it bridges this gap by integrating comprehensive preclinical evaluations of antioxidant, antimicrobial, anticancer, and neuroprotective effects within a unified study framework. Such multi-model preclinical evaluations are rarely integrated into a single study, as prior work has primarily focused on a single bioactivity or on alternative plant sources (Ansari *et al.*, 2024). This fragmentation limits their translational potential due to a lack of broad clinical relevance, biosafety data, or an inclusive assessment of combinatorial efficacy. Conventional selenium treatments, such as sodium selenite, often suffer from narrow therapeutic windows and systemic toxicity, with an oral LD50 as low as 7mg/kg in rats (Ryabova *et al.*, 2024), while chemically synthesized SeNPs may harbor residual impurities or lack natural capping agents, reducing efficacy and increasing side effects (Salem *et al.*, 2022; Behera *et al.*, 2024).

In the veterinary sector, several studies have focused on using selenium nanoparticles fabricated from various sources, e.g., resveratrol, propolis extract and curcumin (Wali, 2019; Abo Zaid *et al.*, 2021; Lajmiri *et al.*, 2024; Awad *et al.*, 2025), as a neuroprotective agent in rats. The central hypothesis of this study is that *Citrus sinensis* peel extracts, rich in bioactive flavonoids, will function as dual reducing and stabilizing agents, producing SeNPs with enhanced biodistribution and superior therapeutic indices compared to conventional treatments. Importantly, veterinary focus remains scarce in the literature on selenium nanoparticles, making this work valuable for the animal health sector, where oxidative stress, infections, cancers, and neurodegenerative disorders pose economic and welfare challenges. Rather than viewing this solely as a synthesis method, the rationale for this work lies in the convergence of sustainable nanotechnology and biomedicine. By leveraging agro-waste valorization, this study aims to develop biocompatible nanoplatforms to address urgent health concerns. To validate this, we employed an integrated experimental design assessing efficacy across four distinct rat models: CCl_4-induced oxidative stress, bacterial wound infection, DMH-induced colon cancer, and STZ-induced Alzheimer's disease. This comprehensive approach contributes novel knowledge and practical pathways toward veterinary therapeutics, catalyzing future research focused on safety profiling and pharmaceutical formulation.

MATERIALS AND METHODS

Preparation of *Citrus sinensis* aqueous peel extract: To prepare the extract, the peels were thoroughly washed with distilled water to remove impurities, shade-dried at 40–45°C for 72 hours until crisp, and ground into a fine powder. Forty grams (40g) of the powdered peel were suspended in 400mL of distilled water (pH 6.5, 25ºC) in sealed Erlenmeyer flasks to prevent evaporation, maintaining a 1:10 (w/v) ratio. The mixture was subjected to agitation using an orbital shaker at 120rpm and 50°C for 90 minutes. Following extraction, the suspension was filtered through Whatman No. 1 filter paper to separate the supernatant from solid residues. The filtrate was subsequently concentrated using a rotary evaporator (BUCHI, Germany) at 50°C under reduced pressure (~200 mbar) to yield a viscous aqueous extract, which was stored at 4°C until further use (Ashraf *et al.*, 2024).

Detection of the active compounds using LC-MS: The detection and identification of active compounds in *Citrus sinensis* peel aqueous extracts using LC-MS involve optimized chromatographic and mass spectrometric conditions to ensure high sensitivity and resolution. Following Ashraf *et al.* (2024) with some modifications, the ultra-performance liquid chromatography (UPLC) was

performed with a C18 reversed-phase column (2.1×100mm, 1.7µm particle size) maintained at 40°C. The mobile phase consisted of solvent A (0.1% formic acid in water) and solvent B (acetonitrile with 0.1% formic acid), delivered using a gradient elution starting from 5% B to 95% B over 20 minutes, then held for 3 minutes. The flow rate was set at 0.3mL/min. Injection volume was 5µL. The mass spectrometer operated with an electrospray ionization (ESI) source in both positive and negative ion modes. The source temperature was maintained at 350°C with a desolvation gas flow of 800L/h. Capillary voltage was set to 3.0kV in positive mode and 2.5kV in negative mode. The scan range was m/z 100–1200 with high-resolution acquisition enabled (Munir *et al.*, 2024).

Synthesis and characterization of Cs-SeNPs: Typically, aqueous peel extract was mixed with a sodium selenite (Na_2SeO_3, 12mM) solution under controlled conditions. Following Dang-Bao *et al.* (2022) with some modification, 20mL of freshly prepared aqueous *C. sinensis* peel extract was added dropwise to 20mL of 10mM sodium selenite solution and incubated at 60°C with continuous stirring for 4 hours. The formation of SeNPs was initially indicated by a noticeable change in color from pale yellow to deep red/orange, confirming the reduction of selenite ions to elemental selenium nanoparticles.

Characterization of the synthesized SeNPs commonly includes UV–visible spectroscopy, in which a characteristic surface plasmon resonance peak is observed at 260–300nm, confirming nanoparticle formation. Transmission electron microscopy (TEM) reveals primarily spherical nanoparticles, often ranging in size from 20 to 80nm. Dynamic light scattering (DLS) measurements provide size distribution and zeta potential values that indicate nanoparticle stability in colloidal suspension. These characterization techniques collectively confirm the successful biosynthesis, morphology, size distribution, stability, and surface chemistry of SeNPs synthesized from *Citrus sinensis* peel extract (Azeem and Abd el Megid, 2023).

Biological activities of Cs-SeNPs

Antioxidant activity: The antioxidant activity was conducted following Behera *et al.* (2024) with some modifications. A stock solution of 2,2-diphenyl-1-picrylhydrazyl (DPPH) (≥95%; Sigma-Aldrich, St. Louis, MO, USA) was prepared in methanol (0.1mM). A stock suspension of Cs-SeNPs (1.0mg/mL) was prepared by dispersing the nanoparticles in distilled water and sonicating for 15 minutes to ensure homogeneity. Working concentrations (25, 50, 100, and 150µg/mL) were prepared by diluting the stock solution with distilled water. In separate triplicate test tubes, 1 mL of the DPPH solution was mixed with 1 mL of each SeNP concentration. The mixtures were vortexed gently and incubated in the dark at room temperature (25±2°C) for 30 minutes to prevent photodegradation. After incubation, the absorbance of each reaction mixture was measured spectrophotometrically at 517 nm against a blank (methanol only) using a UV–Vis spectrophotometer (UV-1800, Shimadzu, Japan). The percentage of DPPH radical scavenging activity was calculated using the formula:

$$\% \text{ Antioxidant activity} = \frac{\text{A control} - \text{A sample}}{\text{A control}} \text{x } 100$$

where *A*control is the absorbance of the control and *A*sample is the absorbance of the SeNPs solution

Antibacterial activity: The antibacterial activity of *Citrus sinensis*–derived selenium nanoparticles (Cs-SeNPs) was evaluated using the disc diffusion assay against four pathogenic bacterial isolates: *Bacillus cereus*, Staphylococcus *aureus*, *Escherichia coli*, and *Klebsiella pneumoniae*. All assays were performed in triplicate following (Azeem and Abd el Megid, 2023; Behera *et al.*, 2024) with some modifications. Fresh bacterial cultures were grown overnight in nutrient broth at 37°C and adjusted to the 0.5 McFarland turbidity standard (1.5×10^8 CFU/mL). Mueller-Hinton agar plates were prepared and uniformly inoculated with each bacterial suspension using a sterile swab to create a lawn culture. Sterile paper discs (6 mm diameter) were impregnated with 20µL of Cs-SeNPs suspension at concentrations of 25, 50, 100, and 150µg/mL. Before application, the nanoparticle suspension was sonicated for 5 min to ensure homogeneity. The discs were then dried under laminar airflow. The loaded discs were placed on the inoculated agar surface with adequate spacing. Plates were incubated at 37°C for 18–24 hours under aerobic conditions. After incubation, antibacterial activity was assessed by measuring the inhibition zone diameter (mm) using a calibrated vernier caliper. Control discs containing distilled water (solvent control) and standard antibiotic discs (neomycin) were included as negative and positive controls, respectively, for comparison.

Anticancer activity

Cell culture: Human breast adenocarcinoma (MDA-MB-231; ATCC® HTB-26™) and colorectal carcinoma (HCT-116; ATCC® CCL-247™) cell lines were procured from the American Type Culture Collection (ATCC, Manassas, VA, USA). The cells were maintained in Dulbecco's Modified Eagle's Medium (DMEM) supplemented with 10% fetal bovine serum (FBS) and 1% penicillin-streptomycin. Cultures were incubated at 37°C in a humidified atmosphere containing 5% CO_2.

Cytotoxicity assessment (MTT Assay): The cytotoxic effect of Cs-SeNPs was evaluated using the MTT (3-(4,5-dimethylthiazol-2-yl)-2,5-diphenyltetrazolium bromide) reduction assay. Cells were seeded in 96-well plates at a density of 10^4 cells/well and allowed to adhere overnight, reaching 70–80% confluency at the onset of treatment. Subsequently, cells were treated with varying concentrations of Cs-SeNPs (25, 50, 100, and 150µg/mL) for 24 hours.

After the exposure period, 20µL of MTT solution (5mg/mL in phosphate-buffered saline) was added to each well and incubated for 4 hours at 37°C. Following incubation, the medium was carefully aspirated, and 150µL of dimethyl sulfoxide (DMSO) was added to dissolve the insoluble purple formazan crystals. The plates were shaken gently for 10 minutes to ensure homogeneity. The absorbance was measured at 570nm (with a reference

wavelength of 630nm) using a microplate reader. The cell viability percentage was calculated using the formula:

$$\text{Cell viability (\%)} = \frac{\text{A sample}}{\text{A control}} \text{x}100$$

Where Asample and Acontrol are the absorbance values of treated and untreated cells, respectively.

Antiviral activity

Reparation and cytotoxicity assessment: Selenium nanoparticles (SeNPs) were suspended in sterile PBS and homogenized via sonication for 10–15 minutes, followed by filtration through a 0.22µm syringe filter to ensure sterility and uniform dispersion. Before antiviral evaluation, the cytotoxicity of SeNPs was determined using the MTT assay to establish a non-toxic therapeutic window. TZM-bl and RAW 264.7 cells were seeded at a density of 1×104 cells/well in 96-well plates and incubated for 24 hours. The monolayers were subsequently treated with SeNPs at concentrations of 25, 50, 100, and 150µg/mL for 48 hours. Following incubation, MTT reagent was added, and the resulting formazan crystals were solubilized with DMSO. Absorbance was measured at 570nm to calculate the 50% cytotoxic concentration (CC50), ensuring that subsequent antiviral assays utilized safe dosages.

Evaluation of anti-HIV-1 activity: Antiviral activity against HIV-1 was assessed using the TZM-bl reporter cell line, which expresses luciferase under the control of the HIV-1 LTR promoter. Briefly, the HIV-1 viral stock was pre-incubated with SeNPs at concentrations of 25, 50, 100, and 150µg/mL for 1 hour at 37°C to facilitate direct virucidal interaction. This mixture was then inoculated onto TZM-bl cells (1×104 cells/well) seeded in 96-well black optical plates. After 48 hours of incubation at 37°C in a 5% CO_2 humidified atmosphere, cells were washed with PBS and lysed using a reporter lysis buffer. The addition of a luciferase substrate quantified luciferase activity, and Relative Light Units (RLU) were measured using a luminometer. The percentage of viral inhibition was calculated for each concentration by normalizing the RLU of treated samples to the RLU of untreated virus controls.

Evaluation of anti-norovirus activity: Due to the difficulty of culturing human norovirus, antiviral efficacy was evaluated using the surrogate Murine Norovirus (MNV-1) and RAW 264.7 macrophage cells via a plaque assay. MNV-1 stock (approximately 105 PFU/mL) was mixed at a 1:1 ratio with SeNPs at concentrations of 25, 50, 100, and 150µg/mL and incubated for 1 hour at 37°C. The treated viral suspension was then inoculated onto confluent RAW 264.7 monolayers in 6-well plates and incubated for 1 hour with gentle rocking to allow viral adsorption. The inoculum was subsequently aspirated and replaced with an overlay medium consisting of 1% agarose and 2X MEM to restrict viral spread. After 48 hours, the cells were fixed with 10% formaldehyde and stained with 0.1% crystal violet. Viral plaques were enumerated to determine the Plaque Forming Units (PFU), and efficacy for each concentration was expressed as the log reduction in viral titer compared to controls.

Anti-Alzheimer activity: The acetylcholinesterase (AChE) inhibition activity was assessed using a modified Ellman's method. In a 96-well microplate, a reaction mixture was prepared by mixing 100µL of Cs-SeNPs at varying concentrations (25, 50, 100, and 150µg/mL) with 100µL of AChE enzyme solution (Type VI-S from *Electrophorus electricus*; 0.03U/mL) prepared in 0.1 M phosphate buffer (pH 8.0). The pH of 8.0 was selected as the standard condition for optimal Ellman's reaction kinetics. Following a pre-incubation period of 15 minutes at 37°C, the reaction was initiated by the sequential addition of 100µL of 5,5′-dithiobis-(2-nitrobenzoic acid) (DTNB, 0.3mM) and 100µL of acetylthiocholine iodide (ATCI, 1.5mM), resulting in a total reaction volume of 400µL following the study of (Shahidi *et al.*, 2024). The mixture was gently mixed and incubated at 37°C for 15 minutes. During this period, AChE catalyzed the hydrolysis of ATCI to produce thiocholine, which reacted with DTNB to form 5-thio-2-nitrobenzoate, a yellow compound. The absorbance was immediately measured at 412nm using a 96-well microplate in a SpectraMax i3x microplate reader (Shimadzu, Japan). Decreased absorbance relative to the control (AChE without Cs-SeNPs) indicates AChE inhibition by the nanoparticles. Percentage inhibition is calculated as:

$$\text{\% Inhibition} = \frac{\text{A control} - \text{A sample}}{\text{A control}} \text{x}\,100$$

In *vivo* experiments

Effect of Cs-SeNPs on oxidative stress and liver markers: Experimental Design: Adult male Wistar rats were divided into five groups (n=10 each): Control: Untreated (received vehicle only). Model Control (T1): Intoxicated with carbon tetrachloride (CCl_4) dissolved in olive oil (1:1 v/v) at a dose of 1.0mL/kg, administered intraperitoneally (i.p.) twice weekly. Standard Control (T2): CCl_4 + Ascorbic acid (100 mg/kg/day) administered orally. Low-Dose Cs-SeNPs (T3): CCl_4 + Cs-SeNPs (0.5 mg/kg/day) administered orally. High-Dose Cs-SeNPs (T4): CCl_4 + Cs-SeNPs (1.0 mg/kg/day) administered orally. Treatments were continued for 4 weeks (Table 1 and Fig. 1).

Sample Collection and Preparation: Twenty-four hours after the final administration, rats were sacrificed. Blood samples were collected, allowed to clot, and centrifuged at 3000rpm for 15 min to obtain serum. Liver tissues were excised, rinsed in ice-cold saline, and homogenized (10% w/v) in ice-cold phosphate buffer, pH 7.4. The homogenate was centrifuged at 4000rpm for 10 min at 4°C, and the supernatant was stored at -80°C for biochemical analysis.

Biochemical Analysis: Liver function enzymes (AST, ALT, ALP) and oxidative stress markers (SOD, CAT, GSH, MDA) were quantified using commercially available kits obtained from Biodiagnostic, Cairo, Egypt (Cat. Nos: AST-101, ALT-102, ALP-103, SOD-110, CAT-111, GSH-112, MDA-113), following the manufacturer's standard protocols (Dang-Bao *et al.*, 2022).

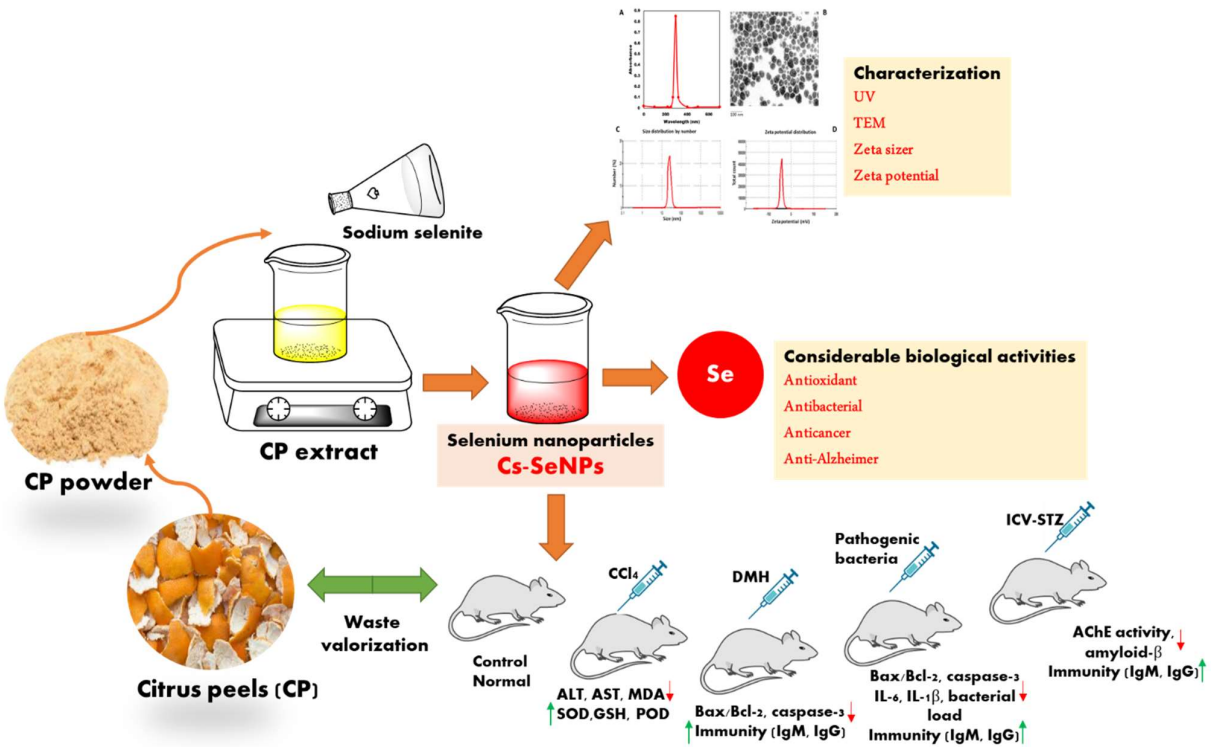

Fig. 1: Schematic representation of the study design and experimental workflow. (A) Green synthesis of selenium nanoparticles (Cs-SeNPs) utilizing *Citrus sinensis* peel (CP) extract as a dual reducing and stabilizing agent for sodium selenite. (B) Physicochemical characterization of the synthesized Cs-SeNPs via UV-Vis spectroscopy, Transmission Electron Microscopy (TEM), and Zeta potential analysis to confirm size and stability. (C) *In vivo* evaluation of the multi-target therapeutic efficacy of Cs-SeNPs across four distinct rat models: CCl_4-induced hepatotoxicity, DMH-induced colon cancer, bacterial wound infection, and ICV-STZ-induced Alzheimer's disease. The schematic highlights key outcomes, including waste valorization, antioxidant restoration, apoptosis induction, antimicrobial activity, and neuroprotection. Abbreviations: CP: Citrus Peels; Se: Selenium; Cs-SeNPs: *Citrus sinensis*-mediated Selenium Nanoparticles; UV: Ultraviolet-Visible Spectroscopy; TEM: Transmission Electron Microscopy; CCl_4: Carbon Tetrachloride; DMH: 1,2-Dimethylhydrazine; ICV-STZ: Intracerebroventricular Streptozotocin; ALT: Alanine Aminotransferase; AST: Aspartate Aminotransferase; MDA: Malondialdehyde; SOD: Superoxide Dismutase; GSH: Reduced Glutathione; POD: Peroxidase; IgM: Immunoglobulin M; IgG: Immunoglobulin G; IL-6: Interleukin-6; IL-1β: Interleukin-1 beta; Bax: Bcl-2-associated X protein; Bcl-2: B-cell lymphoma 2; AChE: Acetylcholinesterase.

Table1: Experimental Design

Group	Animal Model	Treatment	Duration	Parameters Evaluated
Control	Healthy rats	Saline	-	Baseline biochemical & histological values
Antioxidant group	CCl_4-induced oxidative stress	Cs-SeNPs (0.5, 1.0mg/kg) vs Ascorbic acid	21 days	Liver enzymes (AST, ALT, ALP), SOD, CAT, GSH, MDA
Antimicrobial group	Infected wound (*S. aureus, E. coli*)	Cs-SeNPs gel vs Standard antibiotic	14 days	Wound contraction, bacterial load, tissue histology
Anticancer group (DMH)	DMH-induced colon cancer	Cs-SeNPs vs Untreated cancer group	16 weeks	Tumor incidence, multiplicity, histopathology, Bax/Bcl-2, caspase-3
Anticancer group	*E. coli*-induced colon cancer and *K. pneumoniae*-induced colon cancer	Cs-SeNPs vs Untreated bacterial cancer	12 weeks	Tumor incidence, multiplicity, inflammatory markers (IL-1β, NF-κB), bacterial load, Bax/Bcl-2, caspase-3
Anti-Alzheimer group	ICV-STZ induced Alzheimer's	Cs-SeNPs (21 days) vs Donepezil	21 days	Morris water maze, AChE activity, amyloid-β load, oxidative stress markers

Effect of Cs-SeNPs on wound infection and infectious microbes: Experimental Design: Rats were anesthetized via intraperitoneal injection of Ketamine (80 mg/kg) and Xylazine (10mg/kg). To minimize post-operative pain, lidocaine gel (2%) was applied locally at the wound site. Wound Creation and Infection: The rats' dorsal fur was shaved and sterilized with 70% ethanol. A circular full-thickness excisional wound (1.5cm diameter) was created on the dorsum using sterile surgical scissors and forceps. The wounds were immediately inoculated with 50µL of *Staphylococcus aureus* or *Escherichia coli* suspensions (10^8 CFU/mL) and left for 24 hours to establish infection before treatment initiation. Treatment Protocol: Rats were divided into groups and treated once daily for 14 days. Cs-SeNPs Gel Groups: Treated topically with 0.5g of gel containing Cs-SeNPs at concentrations of 0.05% and 0.1% (w/w). Positive Control: Treated with Neosporin ointment (containing Neomycin Sulfate 0.5%). Wound Contraction Measurement: Wound contraction was assessed on days 0, 7, and 14. The wound area was measured by digital photography with a scale reference. The wound area was quantified using ImageJ software (NIH, USA). To prevent bias, the measurements were performed by an investigator blinded to the treatment allocation. The percentage of wound contraction was calculated using the formula:

$$\text{Wound conc} = \frac{\text{Intial area (Day0)} - \text{Specific day area}}{\text{Intial area (Day0)}}$$

Effect of Cs-SeNPs on chemical and pathogen-induced colon cancer: Experimental Design: For chemical carcinogenesis, male Wistar rats received weekly intraperitoneal injections of 1,2-dimethylhydrazine (DMH, 20mg/kg) for 10 weeks (Table 1 and Fig. 1). Bacterial colon cancer was induced by chronic colonization with *Escherichia coli* (ATCC 25922) and *Klebsiella pneumoniae* (ATCC 13883). Cs-SeNPs were administered orally at doses of 0.5 and 1.0 mg/kg three times weekly for a period of 4 weeks and after carcinogen/bacteria exposure. Tumor incidence and multiplicity were recorded post-mortem. Apoptotic markers (Bax, Bcl-2, caspase-3) were quantified by Western blot or ELISA. Pro-inflammatory cytokines (IL-1β, IL-6, TNF-α, NF-κB) were measured in colon tissue homogenates using ELISA kits.

Effect of Cs-SeNPs on Alzheimer's disease: Induction of Alzheimer's Disease: Alzheimer's disease was induced in rats via a single bilateral intracerebroventricular (ICV) injection of streptozotocin (STZ) dissolved in citrate buffer (pH 4.5). Rats were anesthetized and placed in a stereotaxic frame. STZ (3mg/kg) was injected at the following coordinates relative to the bregma: AP: -0.8mm, ML: ±1.5 mm, DV: -3.6mm. The incision was sutured, and the animals were allowed to recover. Treatment Groups: Animals were divided into five groups (n=6): Control: Received ICV injection of citrate buffer only. STZ Control: STZ + Vehicle. Positive Control: STZ + Donepezil (1.0mg/kg). Cs-SeNPs Low Dose: STZ + 0.5mg/kg Cs-SeNPs. Cs-SeNPs High Dose: STZ + 1.0mg/kg Cs-SeNPs. Treatments were administered orally for 21 days starting 24 hours post-surgery.

Cognitive Assessment (Morris Water Maze): Cognitive function was assessed using the Morris water maze (MWM). The apparatus consisted of a circular pool (180 cm diameter, 60cm high) filled with water maintained at 25±1°C. The water was made opaque using non-toxic white paint. The pool was divided into four equal quadrants, with a hidden escape platform (10cm) submerged 1.5 cm below the water surface in the target quadrant.

Acquisition phase: Rats underwent 4 training trials per day for 5 consecutive days. Each trial had a cutoff time of 60 seconds. If the rat failed to locate the platform, it was gently guided to it and allowed to stay for 15 seconds.

Probe trial: On day 6, the platform was removed. Rats were allowed to swim for 60 seconds. The time spent in the target quadrant and the number of platform crossings were recorded using a video tracking system (ANY-maze, Stoelting Co., USA).

AChE activity: Brain acetylcholinesterase (AChE) activity was assessed in tissue homogenates using Ellman's colorimetric method.

Amyloid-β plaque quantification: Brain tissues were fixed in 10% neutral buffered formalin for 24 hours, embedded in paraffin, and sectioned at 5µm. Sections were deparaffinized and stained with Congo Red to visualize amyloid plaques. Images were captured using an Olympus BX53 microscope equipped with a digital camera. The area percentage of amyloid-β plaques was quantified using ImageJ (NIH, USA) software by analyzing 5 random fields per section (Shahidi *et al.*, 2024; Vicente-Zurdo *et al.*, 2024).

Effect of Cs-SeNPs on immunity in wistar rats: Wistar rats were subjected to chronic restraint stress to induce immunosuppression. Treatment groups received Cs-SeNPs at 0.5 or 1.0mg/kg orally for 4 weeks. Total and differential leukocyte counts were determined from blood smears stained with Leishman's stain.

Humoral immunity: Serum IgG and IgM levels were quantified using commercial ELISA kits (Abcam, Cambridge, UK; Cat. No. ab133046). Serum was separated by centrifugation at 3000rpm for 15 min and diluted 1:150 before analysis. The assay was performed according to the manufacturer's protocol, with a detection range of 0.5–200ng/mL, and absorbance was measured at 450nm.

Phagocytic activity: The phagocytic index was assessed using the carbon clearance assay. Rats were injected intravenously via the tail vein with Indian ink (Higgins Black Magic, USA) at a dose of 0.1mL/100g bw. Blood samples were collected from the retro-orbital plexus at 2- and 10-minutes post-injection. The samples were lysed in 0.1% sodium carbonate, and optical density (OD) was measured spectrophotometrically at 675nm. The phagocytic index (K) was calculated using the formula:

$$K = \frac{\ln OD1 - \ln OD2}{t2 - t1}$$

Organ Indices: Spleen and thymus weights were recorded immediately after sacrifice. Organ immune indices were calculated as the ratio of organ weight to body weight (mg/g).

Statistical analysis: All data are expressed as Mean ± Standard Deviation (SD) for n =10 rats per group. Statistical analysis was performed using SPSS (v23). The normality of the data was assessed using the Shapiro-Wilk test. For comparisons across multiple groups, a one-way analysis of variance (ANOVA) was employed, followed by Tukey's post-hoc test for pairwise comparisons. A p-value of less than 0.05 was considered statistically significant. The specific significance levels are denoted in the tables as follows: *P<0.05, **P<0.01, ***P<0.001 versus the disease control group.

RESULTS

Phytochemical profiling of *Citrus sinensis* peel extract: Quantitative LC-MS analysis identified flavanones as the predominant compound class in the *Citrus sinensis* peel extract. Hesperidin was the most abundant bioactive constituent, with a concentration of 12,500±950µg/g, followed by Naringin (4,850±420µg/g) and Neohesperidin (2,150±180µg/g). Significant quantities of polymethoxy flavones (PMFs), specifically Nobiletin (850±75µg/g) and Tangeretin (420±38µg/g), were also detected, alongside phenolic acids such as Chlorogenic acid and Ferulic acid (Table 2).

Characterization of Cs-SeNPs: The synthesis of selenium nanoparticles (Cs-SeNPs) was confirmed by UV-Vis spectroscopy, which exhibited a distinct surface plasmon resonance peak at 280nm. Transmission Electron Microscopy (TEM) analysis revealed that the particles were predominantly spherical with a uniform size distribution. Dynamic Light Scattering (DLS) measurements indicated an average hydrodynamic diameter of ~25nm. The zeta potential distribution showed a surface charge of approximately -22mV, indicating the colloidal stability of the synthesized nanoparticles (Fig. 2).

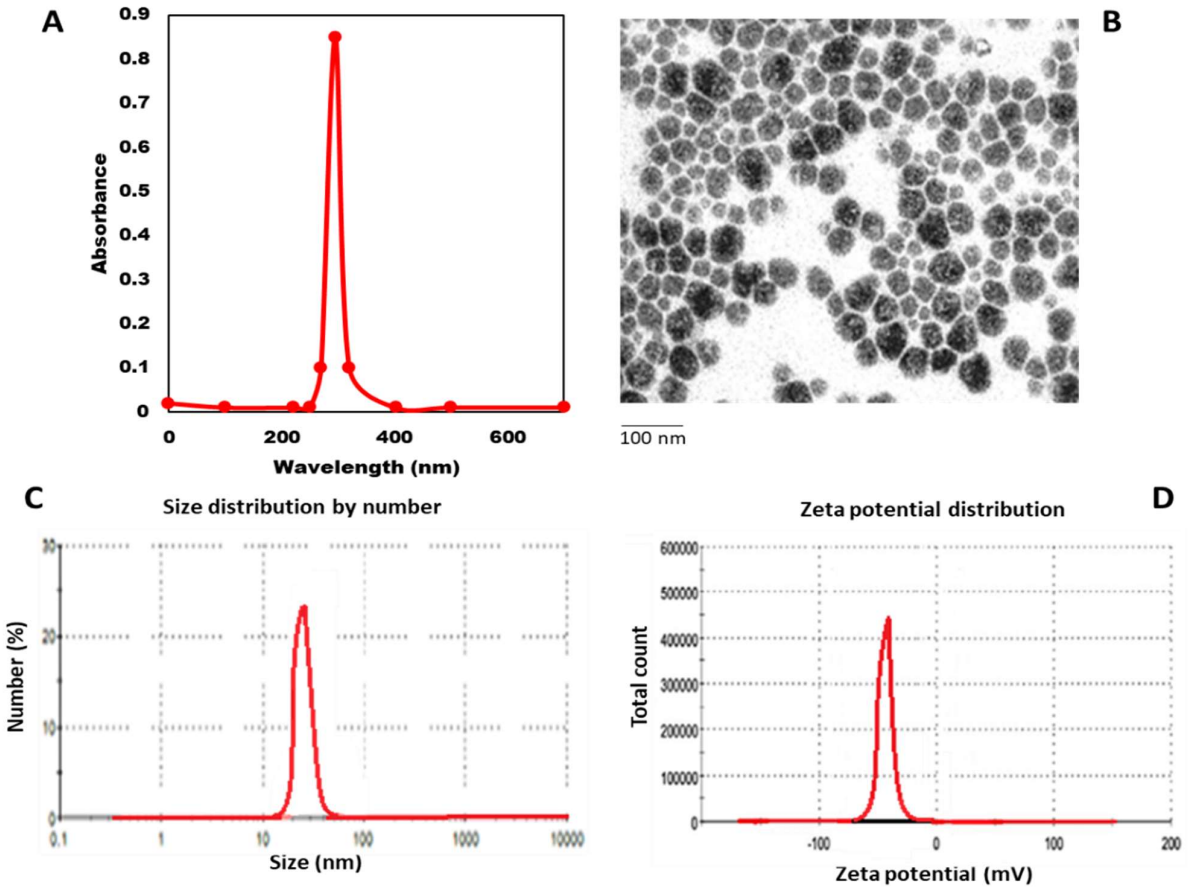

Fig. 2: Characterization of selenium nanoparticles fabricated by *Citrus sinensis* Peel Extract A) UV–Vis absorption spectrum showing a pronounced surface plasmon resonance peak at ~300nm, confirming nanoparticle formation. B) Transmission electron microscopy image revealing predominantly spherical SeNPs with uniform size distribution (scale bar = 100nm). C) Dynamic light scattering size distribution by number, indicating an average hydrodynamic diameter of ~25nm. D) Zeta potential distribution demonstrating a surface charge of approximately -22mV, indicative of colloidal stability.

Table 2: Quantitative LC-MS analysis of major bioactive compounds in *Citrus sinensis* peel extract

Compound Class	Compound Name	Molecular Formula	Retention Time (min)	$[M-H]^-$ or $[M+H]^+$ (m/z)	Concentration (µg/g dry weight) (Mean ± SD)
Flavanones					
	Hesperidin	$C_{28}H_{34}O_{15}$	12.5	609.181 $[M-H]^-$	12500±950
	Naringin	$C_{27}H_{32}O_{14}$	11.8	579.171 $[M-H]^-$	4850±420
	Neohesperidin	$C_{28}H_{34}O_{15}$	13.2	609.181 $[M-H]^-$	2150±180
	Eriocitrin	$C_{27}H_{32}O_{15}$	10.5	595.166 $[M-H]^-$	1850±150
Polymethoxyflavones (PMFs)					
	Nobiletin	$C_{21}H_{22}O_8$	18.7	403.139 $[M+H]^+$	850±75
	Tangeretin	$C_{20}H_{20}O_7$	19.5	373.128 $[M+H]^+$	420±38
	Sinensetin	$C_{20}H_{20}O_7$	17.9	373.128 $[M+H]^+$	280±25
Phenolic acids					
	Ferulic acid	$C_{10}H_{10}O_4$	8.2	193.050 $[M-H]^-$	155±15
	p-Coumaric acid	$C_9H_8O_3$	7.5	163.040 $[M-H]^-$	120±12
	Caffeic acid	$C_9H_8O_4$	6.8	179.035 $[M-H]^-$	95±9
	Sinapic acid	$C_{11}H_{12}O_5$	8.9	223.061 $[M-H]^-$	65±7
Hydroxycinnamic acids					
	Chlorogenic acid	$C_{16}H_{18}O_9$	9.5	353.087 $[M-H]^-$	380±32
Other compounds					
	Ascorbic Acid (Vitamin C)	$C_6H_8O_6$	3.5	175.025 $[M-H]^-$	1050±90
	Limonin	$C_{26}H_{30}O_8$	16.8	469.196 $[M-H]^-$	710±65
	Nomilin	$C_{28}H_{34}O_9$	15.3	469.196 $[M-H]^-$	312±32

Data presented as Mean±Standard Deviation (SD) of triplicate measurements (n=3). Concentrations are expressed as µg/g of dry peel weight.

In Vitro biological activities

Antioxidant activity: Cs-SeNPs demonstrated dose-dependent antioxidant activity. At the highest concentration (150µg/ml), the antioxidant percentage reached approximately 88%, which was statistically comparable (P>0.05) to the standard ascorbic acid (AsA) (Fig. 3).

Antibacterial activity: The disc diffusion assay showed significant growth inhibition against *B. cereus*, *S. aureus*, *E. coli*, and *K. pneumoniae*. The 150µg/mL concentration of Cs-SeNPs exhibited inhibition zones ranging from 22 mm to 35mm, showing efficacy comparable to the standard antibiotic Neomycin against *S. aureus* and *B. cereus* (Fig. 4).

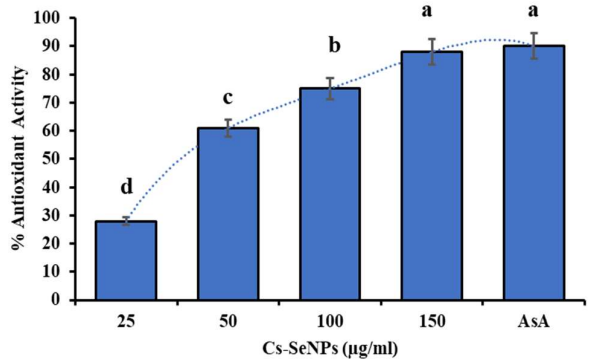

Fig. 3: Dose-dependent antioxidant activity of Cs-SeNPs compared to ascorbic acid. a-d lowercase letters above columns indicate significant differences at P<0.05 between the antioxidant activity of Cs-SeNPs concentrations compared to ascorbic acid (AsA).

Cytotoxicity: Morphological assessment of MDA-MB-231 (breast cancer) and HCT-116 (colon cancer) cell lines treated with Cs-SeNPs revealed distinct signs of apoptosis. Compared to spindle-shaped, confluent control cells, treated MDA-MB-231 cells showed rounded bodies and membrane blebbing. Similarly, treated HCT-116 cells exhibited loss of adhesion, shrinkage, and the formation of apoptotic bodies (Fig. 5).

Cytotoxicity assessment of SeNPs: The MTT assay revealed a concentration-dependent cytotoxic effect of SeNPs on both TZM-bl and RAW 264.7 cell lines. The calculated 50% cytotoxic concentration (CC_{50}) was >150µg/mL for both cell lines, as cell viability remained above 70% at the highest tested concentration (150µg/mL). Based on these results, all subsequent antiviral assays were conducted using the non-toxic concentration range of 25–150µg/mL (Table 3).

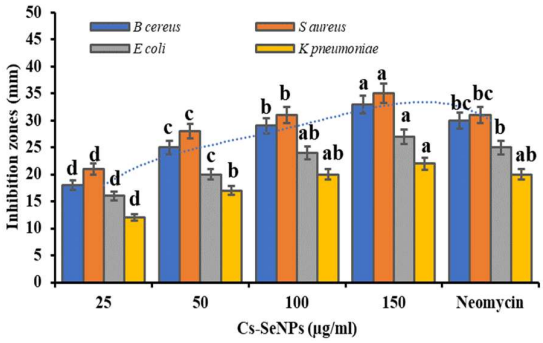

Fig. 4: Antibacterial activity of Cs-SeNPs against pathogenic bacteria. Lowercase letters above columns indicate significant differences at P<0.05.

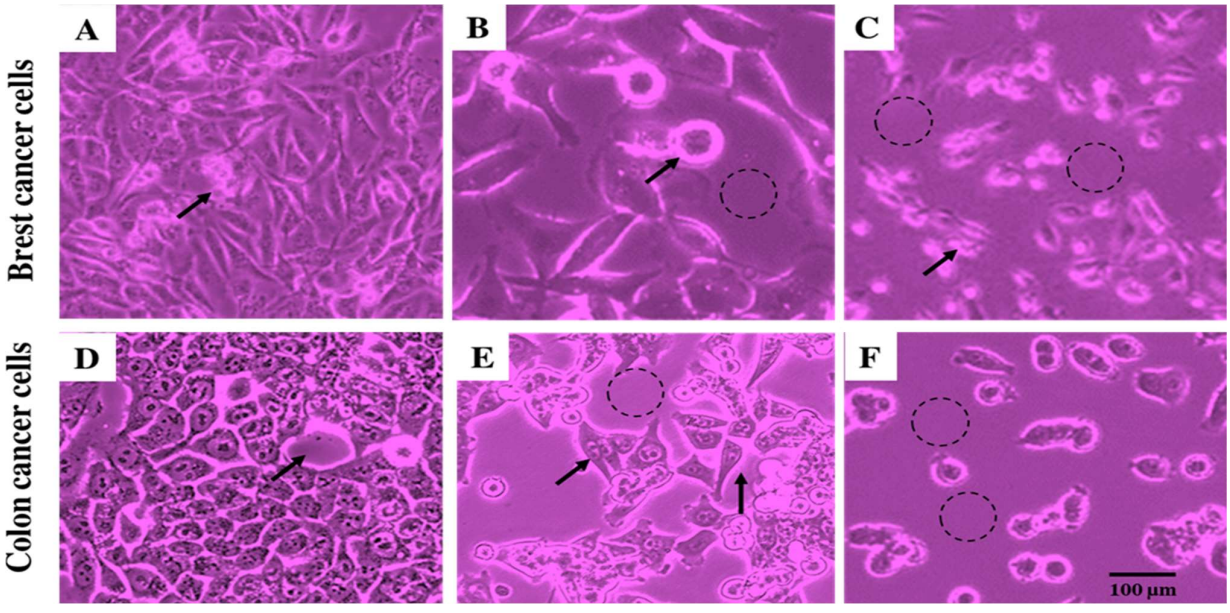

Fig. 5: Cytotoxicity effects of doxorubicin and Cs SeNPs on breast and colon cancer cell lines. A) Untreated MDA MB 231 breast cancer cells exhibit spindle shaped morphology with high confluence and elongated processes. B) MDA MB 231 cells treated with doxorubicin (1 µg/mL) show decreased cell density, rounding, loss of cell–cell contacts, and membrane blebbing, consistent with apoptotic damage. C) MDA MB 231 cells exposed to Cs SeNPs (50 µg/mL) display marked reduction in confluence, cellular rounding, and formation of apoptotic-like bodies, indicating loss of viability. D) Untreated HCT 116 colon cancer cells present polygonal, tightly packed epithelial-like morphology with intact cell–cell junctions. E) HCT 116 cells treated with doxorubicin show pronounced loss of adhesion, membrane blebbing, and cytoplasmic condensation, indicative of advanced apoptosis. F) HCT 116 cells exposed to Cs SeNPs (50 µg/mL) demonstrate reduced cell density, cellular shrinkage, and appearance of apoptotic bodies, reflecting significant cytotoxicity.

Table 3: Cytotoxicity of SeNPs on TZM-bl and RAW 264.7 Cell Lines

SeNP Concentration (µg/mL)	TZM-bl Cell Viability (%±SD)	RAW 264.7 Cell Viability (%±SD)
0 (Control)	100.0±5.2	100.0±4.8
25	98.5±4.1	99.1±5.6
50	95.2±3.7	96.8±4.3
100	88.4±5.9	85.7±6.1
150	72.3±7.2	74.5±5.8

Data presented as Mean±Standard Deviation (SD)

Anti-HIV-1 activity: Pre-incubation of HIV-1 with SeNPs resulted in a significant, dose-dependent reduction in viral infectivity, as measured by luciferase activity in TZM-bl reporter cells. The maximum inhibition of 92.4±3.1% was observed at the highest non-toxic concentration of 150µg/mL. The 50% inhibitory concentration (IC_{50}) was calculated to be 58.7±4.3µg/mL. This resulted in a high selectivity index (SI = CC_{50}/IC_{50}) of >2.6, indicating a favorable therapeutic window for anti-HIV-1 activity (Table 4).

Table 4: Inhibition of HIV-1 by SeNPs in TZM-bl Cells

SeNP Concentration (µg/mL)	% Viral Inhibition (± SD)	Relative Light Units (RLU, % of Control)
0 (Virus Control)	0.0±0.0	100.0±8.5
25	35.2±6.8	64.8±5.9
50	67.8±5.1	32.2±4.2
100	84.5±4.3	15.5±3.7
150	92.4±3.1	7.6±2.8

Data presented as Mean±Standard Deviation (SD)

Anti-norovirus (MNV-1) activity: The plaque reduction assay demonstrated potent virucidal activity of SeNPs against murine norovirus (MNV-1). Pre-treatment of the viral stock with SeNPs led to a significant, dose-dependent decrease in plaque-forming units (PFU). At 150 µg/mL, SeNPs achieved a >3 $\log_{10}$ reduction (99.9% inhibition) in viral titer compared to the virus control. The IC_{50} for MNV-1 was determined to be 41.2±3.8µg/mL (Table 5).

Table 5: Inhibition of Murine Norovirus (MNV-1) by SeNPs in RAW 264.7 Cells

SeNPs Concentration (µg/mL)	Plaque Count (PFU/mL±SD)	Log_{10} Reduction	% Viral Inhibition (± SD)
0 (Virus Control)	$(1.2±0.3) \times 10^5$	0.0	0.0±0.0
25	$(5.8±0.9) \times 10^4$	0.31	51.7±4.5
50	$(1.1±0.4) \times 10^4$	1.04	90.8±3.2
100	$(8.5±2.1) \times 10^2$	2.15	99.3±0.5
150	< 10 (Limit of Detection)	>3.0	>99.9

Data presented as Mean ± Standard Deviation (SD).

AChE inhibition: Cs-SeNPs inhibited: Acetylcholinesterase (AChE) activity in a dose-dependent manner. The 150µg/mL concentration achieved approximately 78% inhibition, which was not significantly different from the standard drug Donepezil (*Fig.* 6).

***In Vivo* hepatoprotective activity**: In the CCl_4-induced hepatotoxicity model, the positive control group (T1) exhibited significantly elevated liver enzymes (AST: 185.7 U/L, ALT: 162.4 U/L) and lipid peroxidation (MDA: 12.5 nmol/mg) compared to the healthy control. Treatment with high-dose Cs-SeNPs (1.0mg/kg, T4) significantly reduced AST (65.3U/L) and ALT (60.2U/L) levels (P<0.001). Furthermore, the T4 group showed restoration of antioxidant markers, with SOD levels increasing to 11.2 U/mg protein and GSH to 23.5nmol/mg protein, values close to the healthy control baseline (Table 6).

Table 6: Effects of Cs-SeNPs on Liver Function and Oxidative Stress Markers in CCl_4-Induced Toxicity in Wistar rats model

Parameter	Control	T1	T2	T3	T4
Liver Function					
AST (U/L)	45.2±4.1	185.7±16.5	75.8±6.9*	95.4±8.7*	65.3±6.0*
ALT (U/L)	38.5±3.8	162.4±14.8	70.1±6.5*	88.7±8.1*	60.2±5.5*
ALP (U/L)	85.3±7.2	210.5±18.9	110.2±10.1*	135.6±12.5*	95.8±8.8*
Oxidative Stress Markers					
SOD (U/mg protein)	12.5±1.2	4.2±0.5	9.8±1.0*	7.5±0.8*	11.2±1.1*
CAT (U/mg protein)	65.4±6.1	18.3±2.1	50.1±4.9*	40.5±4.0*	60.8±5.9*
GSH (nmol/mg protein)	25.8±2.5	8.4±1.0	20.1±2.0*	16.8±1.6*	23.5±2.3*
MDA (nmol/mg protein)	1.8±0.2	12.5±1.4	4.5±0.5*	5.8±0.6*	3.1±0.3*

T1, CCl_4-treated rats; T2, CCl_4 + Ascorbic Acid (100 mg/kg)-treated rats; T3, CCl_4 + Cs-SeNPs (0.5mg/kg)- treated rats; and T4, CCl_4 + Cs-SeNPs (1.0mg/kg)-treated rats**:** Data presented as Mean±SD (n=10 rats/group). *P<0.001 vs. CCl_4 group

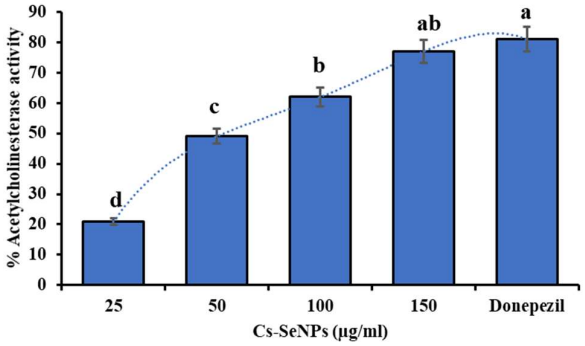

Fig. 6: Dose-dependent inhibition of acetylcholinesterase activity by Cs-SeNPs in ICV-STZ-Induced Alzheimer's model compared to Donepezil. Lowercase letters above columns indicate significant differences at P<0.05.

Antimicrobial efficacy in wound healing: In the infected wound model, the untreated infected control group showed limited wound contraction (65.8%) and a high bacterial load (5.1 Log10 CFU/g) by day 14. Conversely, treatment with 1.0mg/kg Cs-SeNPs gel resulted in 99.2% wound contraction and a reduction in bacterial load to 0.4 Log10 CFU/g, demonstrating statistical superiority over the untreated control (P<0.001) and comparable efficacy to the standard antibiotic gel (Table 7).

Table 7: Antimicrobial effects of Cs-SeNPs on wound infection model

Group	Treatment	Wound Contraction (%)		Bacterial Load (Log_{10} CFU/g)	
		Day 7	Day 14	Day 7	Day 14
1. Uninfected Control	Base Gel	58.2±5.3	99.5±1.2	0±0	0±0
2. Infected Control	Base Gel	25.4±3.1	65.8±6.6	8.2±0.7	5.1±0.5
3. Infected + Standard Antibiotic	Neomycin/ SSD Gel	45.7±4.5*	92.3±3.5*	4.1±0.4*	1.8±0.2*
4. Infected + Cs-SeNPs Gel	0.5 mg/kg	55.8±5.2*	97.8±2.1*	3.0±0.3*	0.9±0.1*
5. Infected + Cs-SeNPs Gel	1.0 mg/kg	68.5±6.1*	99.2±0.9*	1.5±0.2*	0.4±0.05*

Excisional wound infected with *S. aureus* and *E. coli.* Treatment: Topical application of Cs-SeNPs gel. Wound contraction data as Mean %±SD (n=10 rats/group). Bacterial load data as Mean Log_{10} CFU/g tissue±SD. P<0.001 vs. Infected Control group.

Table 8: Anticancer effects of Cs-SeNPs on chemically-induced and bacteria-associated colon cancer models

Group	Induction Model	Dose (mg/kg)	Tumor Data		Apoptosis genes		Inflammation genes			
			Incidence (%)	Multiplicity	Bax/Bcl-2 Ratio	Caspase-3	IL-1β	IL-6 (pg/mg)	TNF-α	NF-κB
Control	-	-	0	0±0	1.0±0.1	1.0±0.1	12.5±1.2	15.2±1.8	8.2±0.8	1.0±0.1
DMH Control	Chemical (DMH)	-	100	5.2±0.6	0.3±0.05	0.4±0.05	-	-	-	-
Infected Control	Bacterial	-	90	3.8±0.5	-	-	125±9.2	85.4±8.1	95±5.2	5.2±0.6
Std. Drug	Chemical (DMH)	25	40	1.8±0.2*	3.0±0.3*	3.2±0.3*	-	-	-	-
Std. Drug	Bacterial	25	55	2.2±0.3*	-	-	52±5.6*	70.1±6.9*	78.5±7.1*	3.5±0.1*
Cs-SeNPs	Chemical (DMH)	0.5	50	2.5±0.3*	2.2±0.2*	2.5±0.3*	-	-	-	-
Cs-SeNPs	Bacterial	0.5	60	2.5±0.3*	-	-	41±3.3*	55.8±5.5*	51±3.6*	2.5±0.2*
Cs-SeNPs	Chemical (DMH)	1.0	30*	1.0±0.2*	5.2±0.5*	5.5±0.6*	-	-	-	-
Cs-SeNPs	Bacterial	1.0	35*	1.2±0.2*	-	-	30±2.2*	35.5±3.6*	40±3.5*	1.1±0.1*

Model A (Chemical): Dimethylhydrazine (DMH)-induced colon carcinogenesis; Model B (Bacterial): Chronic infection with *E. coli* and *K. pneumoniae* to induce inflammatory-driven carcinogenesis. Data presented as Mean±SD (n=10 rats/group). P<0.001 vs. respective control group (DMH or Infected Control). DMH (Dimethylhydrazine), Std. (Standard), 5-FU (5-Fluorouracil, assumed standard drug), CFU (Colony Forming Units), IL-6 (Interleukin-6). (-) indicates that the parameter was not measured or is not applicable for that specific experimental model.

Anticancer efficacy (colon cancer models)

Tumor incidence: In the DMH-induced chemical model, tumor incidence decreased from 100% in the untreated group to 30% in the high-dose Cs-SeNP group (1.0 mg/kg). Similarly, in the bacterial-induced model, incidence dropped from 90% to 35% with treatment.

Apoptosis markers: Cs-SeNPs treatment (1.0mg/kg) significantly upregulated the Bax/Bcl-2 ratio to 5.2 in the DMH model compared to 0.3 in the disease control (Table 8).

Inflammatory markers: In the bacterial-induced cancer model, Cs-SeNPs significantly reduced inflammatory cytokines. IL-6 levels dropped from 85.4pg/mg in the infected control to 35.5pg/mg in the treated group, and NF-κB levels decreased from 5.2 to 1.1.

Anti-Alzheimer's activity: Induction of Alzheimer's via ICV-STZ resulted in a significant increase in escape latency (58.7 s) and brain AChE activity (95.8 nmol/min/mg) compared to the sham control. Treatment with Cs-SeNPs (1.0mg/kg) significantly reduced escape latency to 22.5 s and inhibited AChE activity to 52.7 nmol/min/mg. Additionally, amyloid-beta plaque load was reduced from 22.4% in the disease model to 9.0% in the high-dose treatment group (Table 9).

Table 9: Anti-Alzheimer's effects on ICV-STZ induced model

Group	Dose (mg/kg)	Escape Latency (s)	AChE Activity (nmol/min/mg protein)	Amyloid-Beta Plaque Load (%)
1. Sham Control	-	15.2±2.1	45.5±4.2	1.5±0.3
2. ICV-STZ	-	58.7±6.5	95.8±8.9	22.4±2.5
3. ICV-STZ + Donepezil (Std.)	1.0	25.8±3.0*	60.1±5.8*	12.1±1.4*
4. ICV-STZ + Cs-SeNPs	0.5	35.4±3.8*	75.5±7.1*	15.8±1.7*
5. ICV-STZ + Cs-SeNPs	1.0	22.5±2.5*	52.7±5.0*	9.0±1.0*

Alzheimer's disease induced by intracerebroventricular streptozotocin (ICV-STZ). Cs-SeNPs administered for 21 days. Behavioral data as Mean ± SD (n=10 rats/group). Biochemical data as MEAN ± SD from brain homogenate. P<0.001 vs. ICV-STZ group.

Immunomodulatory effects: Chronic stress induced leukocytosis ($15.8x10^3$µL), lymphopenia (45.2%), and thymus atrophy (1.3 mg/g index) in the control group. Administration of Cs-SeNPs (1.0mg/kg) normalized the total WBC count to 9.8 $x10^3$µL and restored lymphocyte percentages to 63.8%. Humoral immunity was also enhanced, with IgG levels recovering from 85.4 mg/dL in the stressed group to 120.8mg/dL in the treated group (Table 10).

Table 10: Immunomodulatory effects of Cs-SeNPs in a rat models

Immune Parameter	Control (Healthy)	Stressed Control	Stressed + Cs-SeNPs (0.5 mg/kg)	Stressed + Cs-SeNPs (1.0 mg/kg)	Standard
Cellular Immunity					
WBC Count ($x10^3$/µL)	8.5±0.9	15.8±1.6 (Leukocytosis)	12.2±1.3*	9.8±1.0*	11.5±1.2*
Lymphocyte Count (%)	65.4±6.5	45.2±4.8 (Lymphopenia)	55.1±5.6*	63.8±6.4*	58.3±5.9*
Neutrophil Count (%)	25.8±2.8	48.5±5.1 (Neutrophilia)	36.2±3.8**	28.5±3.0*	33.8±3.5**
Humoral Immunity					
IgG (mg/dL)	125.5±12.8	85.4±8.9 (Suppressed)	105.8±10.7*	120.8±12.2*	110.5±11.2*
IgM (mg/dL)	32.5±3.5	20.1±2.2 (Suppressed)	25.8±2.7*	30.2±3.1*	26.5±2.8*
Phagocytic Activity					
Phagocytic Index (%)	68.5±7.1	40.2±4.2 (Suppressed)	55.8±5.7*	65.2±6.6*	58.5±6.0*
Organ Weight Index					
Spleen Index (mg/g)	2.5±0.3	4.2±0.5 (Splenomegaly)	3.2±0.3*	2.8±0.3*	3.4±0.4*
Thymus Index (mg/g)	2.2±0.2	1.3±0.1 (Atrophy)	1.8±0.2*	2.0±0.2*	1.7±0.2*

Wistar rats were treated with Cs-SeNPs across various disease models (Oxidative Stress, Infection, Cancer, Alzheimer's). Key immune parameters were measured from serum and tissue homogenates. Data presented as Mean±SD (n=10 rats/group). *P<0.05, **P<0.01, ***P<0.001 vs. respective Disease Control group.

DISCUSSION

The green synthesis of selenium nanoparticles (SeNPs) using *Citrus sinensis* (orange) peel extract is a rapidly advancing area of research, driven by the need for sustainable, biocompatible, and multifunctional nanomaterials. This discussion provides an in-depth comparison of current findings on *Citrus sinensis* peel-derived SeNPs with similar studies utilizing other plant-based extracts, focusing on synthesis, characterization, antioxidant and antimicrobial activities, and broader biomedical potential.

Citrus sinensis peel is rich in flavonoids, polyphenols, tannins, and essential oils, making it an excellent natural reducing and stabilizing agent for nanoparticle synthesis (Liew *et al.*, 2018; Behera *et al.*, 2024; Bagyalakshmi and Prathiksha, 2025). The green synthesis approach eliminates hazardous chemicals, aligning with eco-friendly and sustainable practices. SeNPs synthesized from *Citrus sinensis* peel typically exhibit spherical morphology, with sizes ranging from 18 to 73 nm, as confirmed by techniques such as UV-Vis, FTIR, XRD, SEM, and TEM (Dang-Bao *et al.*, 2022; Behera *et al.,* 2024). The presence of organic molecules from the peel extract on the nanoparticle surface, confirmed by FTIR,

suggests effective capping and stabilization, which is crucial for biological activity and colloidal stability (Dang-Bao *et al.,* 2022; Behera *et al.,* 2024).

Comparatively, other fruit peels such as pineapple (Ananas comosus) and pomegranate (Punica granatum) have also been used for SeNPs synthesis, yielding nanoparticles with similar size ranges and stability (Hashem *et al.*, 2023; Soliman and Salem, 2025). For example, pineapple peel-derived SeNPs were found to be 33–73nm in size, while pomegranate peel SeNPs averaged 14.5nm (Hashem *et al.,* 2023; Soliman and Salem, 2025). The choice of plant extract influences not only the size and shape but also the surface chemistry and, consequently, the biological properties of the nanoparticles.

Citrus sinensis peel-derived SeNPs consistently demonstrate high antioxidant activity, often surpassing that of the peel extract alone and sometimes even standard antioxidants like ascorbic acid (Liew *et al.*, 2018; Behera *et al*., 2024). DPPH radical scavenging activity for *Citrus sinensis* SeNPs can reach up to 88% at 150µg/ml, indicating potent free radical neutralization. This superior activity is attributed to the synergistic effects of selenium and the surface-bound phytochemicals, particularly flavonoids and phenolic acids (Ogo *et al.*, 2024b).

When compared to SeNPs synthesized from other plant sources, *Citrus sinensis* SeNPs often exhibit equal or greater antioxidant efficacy. *Citrus sinensis* peel extract produced SeNPs with the highest DPPH radical scavenging activity among those synthesized from *Millettia pinnata* and *Acacia auriculiformis* (Behera *et al.,* 2024). Similarly, *Carica papaya*-derived SeNPs showed strong antioxidant activity, with EC50 values of 45–46µg/mL in DPPH and ABTS assays, but *Citrus sinensis* SeNPs still ranked among the most effective (Vundela *et al.*, 2022). The antioxidant capacity is closely linked to the phytochemical composition of the extract, with higher total phenolic and flavonoid content correlating with greater activity (Liew *et al.,* 2018; Ogo *et al.,* 2024b).

Citrus sinensis SeNPs exhibit broad-spectrum antibacterial activity against both Gram-positive and Gram-negative bacteria, including antibiotic-resistant strains (Alvi *et al.*, 2021; Dang-Bao *et al.,* 2022). Inhibition zones for Citrus sinensis SeNPs range from 20 to 35mm, with minimum inhibitory concentrations (MICs) as low as 4.94µg/L against methicillin-resistant Staphylococcus aureus (MRSA) (Dang-Bao *et al.,* 2022). These results are comparable to, and sometimes exceed, those of standard antibiotics like ciprofloxacin (Alvi *et al.,* 2021; Dang-Bao *et al.,* 2022).

Other plant-based SeNPs, such as those from pomegranate and pineapple peels, also show strong antibacterial activity. Pomegranate peel SeNPs produced inhibition zones up to 54mm against *Streptococcus mutans* and demonstrated efficacy against a range of pathogens (Hashem *et al.,* 2023). Pineapple peel SeNPs inhibited *S. aureus, E. coli, B. subtilis, E. faecalis,* and *K. pneumoniae*, with notable antibiofilm activity and suppression of virulence genes (Soliman and Salem, 2025).

However, SeNPs synthesized from Zambian medicinal herbs showed only mild activity against *S. aureus* and none against *E. coli*, highlighting the importance of the plant source and synthesis conditions (Chilala *et al.*, 2025). The mechanism of antimicrobial action involves disruption of bacterial membranes, generation of reactive oxygen species, and interference with biofilm formation and virulence gene expression (Alvi *et al.,* 2021). The presence of surface-bound phytochemicals enhances these effects, making *Citrus sinensis* SeNPs particularly potent.

Citrus sinensis SeNPs have demonstrated selective cytotoxicity against cancer cell lines, inducing apoptosis and reducing tumor incidence in *vivo* (Vundela *et al.,* 2022; Ogo *et al.,* 2024b). IC50 values for *Citrus sinensis* SeNPs are typically in the low µg/mL range, indicating strong anticancer potential. For example, pomegranate peel SeNPs showed IC50 values of 69.8 and 47.9µg/mL for MCF7 and Mg63 cell lines, respectively (Hashem *et al.,* 2023). Pineapple peel SeNPs had an IC50 of 113µg/mL against HepG2 cells (Soliman and Salem, 2025). *Carica papaya* SeNPs also exhibited preferential toxicity toward cancer cells while sparing normal cells at lower concentrations (Vundela *et al.,* 2022).

The anticancer effects are attributed to the induction of apoptosis, upregulation of pro-apoptotic markers, and suppression of inflammatory cytokines (Ikram *et al.*, 2021). The biocompatibility and hemocompatibility of these nanoparticles are generally high, with minimal toxicity to normal cells and tissues at biologically relevant doses (Hashem *et al.,* 2023).

Citrus sinensis SeNPs have shown the ability to restore liver function and antioxidant status in hepatotoxicity models, reflecting their potential in mitigating oxidative stress and cellular damage (Ikram *et al.,* 2021). Their application in infected wound models has resulted in accelerated healing, reduced bacterial load, and enhanced tissue regeneration, often outperforming standard treatments.

SeNPs from *Citrus sinensis* and other plant sources have demonstrated neuroprotective effects, including inhibition of acetylcholinesterase (AChE) activity and reduction of amyloid-beta plaques in Alzheimer's models (Ikram *et al.,* 2021). Immunomodulatory effects include normalization of leukocyte counts, restoration of lymphocyte percentages, and enhancement of humoral immunity, which are crucial for recovery from chronic stress and infection (Ikram *et al.,* 2021). Several studies have also explored the synthesis of silver nanoparticles (AgNPs) using *Citrus sinensis* peel extract, reporting exceptional antibacterial, antioxidant, and anticancer properties (Chen *et al.*, 2022; Gupta *et al.*, 2025). While AgNPs are effective, SeNPs offer additional benefits such as lower toxicity, better biocompatibility, and unique therapeutic properties related to selenium's biological role (Chen *et al.*, 2023). The efficacy of *Citrus sinensis* SeNPs is influenced by extraction methods, solvent choice, and synthesis conditions. Methanol, ethanol, and acetone extracts yield varying levels of phenolics and flavonoids, which directly impact antioxidant and antimicrobial activities (El-Zayat *et al.*, 2021; Długosz *et al.*, 2023; Sentkowska *et al.*, 2024). Optimal synthesis conditions, such as pH, temperature, and extract-to-precursor ratios, are critical for producing uniform, stable, and bioactive nanoparticles (Behera *et al.,* 2024).

Despite promising results, plant-based SeNPs have yet to achieve widespread adoption in the pharmaceutical

industry, partly due to variability in synthesis protocols, lack of standardization, and limited in vivo studies (Ikram *et al.,* 2021). Future research should focus on optimizing synthesis methods, scaling up production, and conducting comprehensive preclinical and clinical evaluations to fully realize the therapeutic potential of *Citrus sinensis* SeNPs and similar nanomaterials.

Conclusions: *Citrus sinensis* peel-derived selenium nanoparticles represent a highly effective, sustainable, and multifunctional nanomaterial with robust antioxidant, antimicrobial, anticancer, hepatoprotective, neuroprotective, wound healing, and immunomodulatory properties. When compared to similar studies using other plant-based extracts, *Citrus sinensis* SeNPs consistently demonstrate superior or comparable efficacy, largely due to the rich phytochemical profile of the peel and optimized green synthesis methods. Continued research and development in this field hold significant promise for advancing nanomedicine and sustainable biomedical applications.

Authors contribution: Conceptualization**,** AOS, KBHS, MFA, SMAB, AM, SA, and MAA, formal analysis, EOA, AAA, MAA, AKH, FAA, ZRA, and IZ, investigation, AOS, KBHS, MFA, SMAB, AM, SA, and MAA, data curation, EOA, AAA, MAA, AKH, FAAG, ZRA, and IZ, writing original draft preparation, AOS, KBHS, MFA, SMAB, AM, SA, and MAA, writing final manuscript and editing, EOA, AAA, MAA, AKH, FAA, ZRA, and IZ, visualization and methodology, AOS, KBHS, MFA, SMAB, AM, SA, MAA, EOA, AAA, MAA, AKH, FAA, ZRA, and IZ. All authors have read and agreed to the published version of the manuscript.

Acknowledgments: The authors gratefully acknowledge the funding of the Deanship of Graduate Studies and Scientific Research, Jazan University, Saudi Arabia, through Project number: (JU-202505354-DGSSR- ORA - 2025).

Funding: This research was funded by Deanship of Graduate Studies and Scientific Research, Jazan University, Saudi Arabia, through Project number: (JU-202505354-DGSSR- ORA -2025.

Conflict of interest: The authors declare that the research was conducted without any commercial or financial relationships that could be construed as a potential conflict of interest.

REFERENCES

Abo Zaid OR, Aziza S, EL-sonbaty SM, *et al.,* 2021. Selenium nanoparticles coated with resveratrol ameliorates the neurobiochemical abnormalities by attenuating oxidative stress and improving neurotransmissions in $AlCl_3$-Induced Alzheimer's model of rats. Benha Vet Med J 41:173-177.

Alsulami MN, El-Saadony MT, 2024. The enhancing effect of bacterial zinc nanoparticles on performance, immune response, and microbial load of Nile Tilapia (*Oreochromis niloticus*) by reducing the infection by *Trichodina heterodentata*. Pak Vet J 44(3): 599-610.

Alsulami MN, El-Saadony MT, 2023. Supplementing broiler diets with bacterial selenium nanoparticles enhancing performance, carcass traits, blood indices, antioxidant status, and caecal microbiota of Eimeria tenella-infected broiler chickens. Poult Sci 102(12): 103111.

Altammar KA, 2023. A review on nanoparticles: characteristics, synthesis, applications, and challenges. Front Microbiol 14:1155622.

Alvi GB, Iqbal M, Ghaith M, *et al.,* 2021. Biogenic selenium nanoparticles (SeNPs) from citrus fruit have anti-bacterial activities. Sci Rep 11:4811.

Ansari JA, Malik JA, Ahmed S, *et al.*, 2024. Recent advances in the therapeutic applications of selenium nanoparticles. Mol Biol Reports 51:688.

Ashraf H, Iahtisham-Ul-Haq, Butt MS, *et al.,* 2024. Phytochemical and antioxidant profile of citrus peel extracts in relation to different extraction parameters. Int J Food Prop 27:286-299.

Awad SM, Attia YA, ElSayed H, *et al.,* 2025. Efficacy of curcumin-selenium nanoemulsion in alleviating oxidative damage induced by aluminum chloride in a rat model of Alzheimer's disease. J Mol Histol 56:122.

Azeem AA and Abd el Megid MH, 2023. Assessment of the biogenic effects of selenium nanoparticles prepared from citrus paradise peel extract against bisphenol A-Induced liver injury in male rats. Pak J Zool 55:2317.

Bagyalakshmi J and Prathiksha M, 2025. Green synthesis of *Citrus sinensis* peel (Orange peel) extract silver nanoparticle and its various pharmacological activities. Arch Pharm Pharma Sci 2 (1): 009-013.

Behera A, Jothinathan MKD, Ryntathiang I, *et al.,* 2024. Comparative antioxidant efficacy of green-synthesised selenium nanoparticles from *Pongamia pinnata*, *Citrus sinensis*, and *Acacia auriculiformis*: An *In Vitro* analysis. Cureus 16(4):e58439.

Behera A, Jothinathan MKD, Ryntathiang I, *et al.,* 2024. Comparative antioxidant efficacy of green-synthesised selenium nanoparticles from *Pongamia pinnata*, *Citrus sinensis*, and *Acacia auriculiformis*: an in vitro analysis. Cureus 16.

Chen F, Zheng Q, Li X, *et al.,* 2022. *Citrus sinensis* leaf aqueous extract green-synthesized silver nanoparticles: Characterization and cytotoxicity, antioxidant, and anti-human lung carcinoma effects. Arab J Chem 15:103845.

Chen N, Yao P, Zhang W, *et al.,* 2023. Selenium nanoparticles: Enhanced nutrition and beyond. Crit Rev Food Sci Nutr 63:12360-12371.

Chilala P, Jurickova M, Pokorna Z, *et al.,* 2025. Antioxidant properties and antimicrobial activity of selenium nanoparticles synthetized via Zambian medicinal herbs. PLOS One 20(6): e0325460.

Chin S, Moniruzzaman M, Smirnova E, *et al.,* 2024. Green metal nanotechnology in monogastric animal health: current trends and future prospects—A review. Anim Biosci 38(1):19-32.

Dang-Bao T, Ho TG-T, Do BL, *et al.,* 2022. Green orange peel-mediated bioinspired synthesis of nanoselenium and its antibacterial activity against methicillin-resistant *Staphylococcus aureus*. ACS omega 7:36037-36046.

Dang-Bao T, Ho TG-T, Barbe, Anh NP, *et al.,* 2022. Green orange peel-mediated bioinspired synthesis of nanoselenium and its antibacterial activity against methicillin-resistant *Staphylococcus aureus*. ACS Omega 7:36037-36046.

Długosz O, Chmielowiec-Korzeniowska A, Drabik A, *et al.,* 2023. Bioactive selenium nanoparticles synthesized from propolis extract and quercetin based on natural deep eutectic solvents (NDES). J Clust Sci 34:1401-1412.

El-Zayat MM, Eraqi MM, Alrefai H, *et al.,* 2021. The antimicrobial, antioxidant, and anticancer activity of greenly synthesized selenium and zinc composite nanoparticles using *Ephedra aphylla* extract. Biomolecules 11:470.

El-Saadony MT, Saad AM, Sitohy M, *et al.,* 2025. Chitosan nanoparticles: green synthesis, biological activities, and sustainable frontiers in targeted drug delivery and cancer nanomedicine–A comprehensive review. Mat Today Bio 35: 102358.

El-Saadony MT, Fang G, Yan S, *et al.*, 2024. Green synthesis of zinc oxide nanoparticles: preparation, characterization, and biomedical applications-a review. Int J Nanomed 19: 12889-12937.

Gupta S, Choudhary DK and Sundaram S, 2025. Green synthesis and characterization of silver nanoparticles using *Citrus sinensis* (Orange peel) extract and their antidiabetic, antioxidant, antimicrobial and anticancer activity. Waste Biomass Valori 16:1101-1114.

Hashem A, Saied E, Ali O, *et al.,* 2023. Pomegranate peel extract stabilized selenium nanoparticles synthesis: Promising antimicrobial potential, antioxidant activity, biocompatibility, and hemocompatibility. Appl Biochem Biotechnol 195: 5753–5776

Ikram M, Javed B, Raja N, *et al.,* 2021. Biomedical potential of plant-based selenium nanoparticles: A comprehensive review on therapeutic and mechanistic aspects. Int J Nanomed 16:249-268.

Kazemi M, 2025. Revolutionizing veterinary medicine: the role of nanoparticles in advancing animal health, nutrition and disease management. Vet Med Sci 11:e70528.

Lajmiri E, Javdani M, Khosravian P, *et al.,* 2024. Preparation and evaluation of controlled released implant containing mesoporous selenium nanoparticles loaded with curcumin in rats with spinal cord injury. In: Vet Res Forum. 15(7):357-367.

Liew SS, Ho W, Yeap S, *et al.,* 2018. Phytochemical composition and in vitro antioxidant activities of *Citrus sinensis* peel extracts. PeerJ 6:e5331.

Maqbool Z, Khalid W, Atiq HT, *et al.,* 2023. Citrus waste as source of bioactive compounds: Extraction and utilization in health and food industry. Molecules 28:1636.

Munir H, Yaqoob S, Awan KA, *et al.,* 2024. Unveiling the chemistry of citrus peel: Insights into nutraceutical potential and therapeutic applications. Foods 13:1681.

Ogo O, Hembafan N, Amokaha R, *et al.,* 2024a. Characterization and antioxidant activity of peel extracts from three varieties of citrus sinensis. Heliyon 10(7): e28456.

Reda FM, Alagawany M, Salah AS, *et al.,* 2024. Biological selenium nanoparticles in quail nutrition: biosynthesis and its impact on performance, carcass, blood chemistry, and cecal microbiota. Biol Trace Elem Res 202(9): 4191-4202.

Reda FM, El-Saadony MT, Elnesr SS, *et al.,* 2020. Effect of dietary supplementation of biological curcumin nanoparticles on growth and carcass traits, antioxidant status, immunity and caecal microbiota of Japanese quails. Animals 10(5): 754.

Ryabova YV, Sutunkova MP, Minigalieva IA, *et al.,* 2024. Toxicological effects of selenium nanoparticles in laboratory animals: A review. J Appl Toxicol 44:4-16.

Saad AM, Sitohy MZ, Sultan-Alolama MI, *et al.,* 2022. Green nanotechnology for controlling bacterial load and heavy metal accumulation in Nile tilapia fish using biological selenium nanoparticles biosynthesized by *Bacillus subtilis* AS12. Front Microbiol 13: 1015613.

Saini RK, Ranjit A, Sharma K, *et al.,* 2022. Bioactive compounds of citrus fruits: A review of composition and health benefits of carotenoids, flavonoids, limonoids, and terpenes. Antioxidants 11:239.

Salem SS, Badawy MSE, Al-Askar AA, *et al.,* 2022. Green biosynthesis of selenium nanoparticles using orange peel waste: Characterization, antibacterial and antibiofilm activities against multidrug-resistant bacteria. Life 12:893.

Saxena R, Kotnala S, Bhatt S, *et al.,* 2025. A review on green synthesis of nanoparticles toward sustainable environment. Sust Chem Clim Action 6: 100071.

Sentkowska A, Konarska J, Szmytke J, *et al.,* 2024. Herbal polyphenols as selenium reducers in the green synthesis of selenium nanoparticles: Antibacterial and antioxidant capabilities of the obtained SeNPs. Molecules 29:1686.

Shahidi S, Asl SS, Gholamigeravand B, *et al.,* 2024. Effect of mesenchymal stem cells and polyvinyl alcohol-coated selenium nanoparticles on rats with Alzheimer-like phenotypes. Iran J Basic Med Sci 27:1268.

Sheiha AM, Abdelnour SA, Abd El-Hack ME, *et al.,* 2020. Effects of dietary biological or chemical-synthesized nano-selenium supplementation on growing rabbits exposed to thermal stress. Animals 10(3): 430.

Singaravelu S, Motsoene F, Abrahamse H, *et al.,* 2025. Green-synthesized metal nanoparticles: a promising approach for accelerated wound healing. Front Bioeng Biotechnol 13:1637589.

Soliman M, Salem S, 2025. Uncovering the potential of biofabricated Ananas comosus peel selenium nanoparticles for antibacterial, antibiofilm, suppression of virulence genes (can and LuxS), anticancer, and antioxidant properties. BMC Biotechnol 25:51.

Vicente-Zurdo D, Rosales-Conrado N and León-González ME, 2024. Unravelling the in vitro and in vivo potential of selenium nanoparticles in Alzheimer's disease: A bioanalytical review. Talanta 269:125519.

Vundela SR, Kalagatur NK, Nagaraj A, *et al.,* 2022. Multi-biofunctional properties of phytofabricated selenium nanoparticles from *Carica papaya* fruit extract: Antioxidant, antimicrobial, antimycotoxin, anticancer, and biocompatibility. Front Microbiol 12:769891.

Wali AT, 2019. Biosynthesis, characterization and bioactivity of selenium nanoparticles synthesized by propolis: 1Ahmed Thamer Wali1 and 2Majida AJ Alqayim. Iraqi J Vet Med 43:197-209.

Ying S, Guan Z, Ofoegbu PC, *et al.,* 2022. Green synthesis of nanoparticles: Current developments and limitations. Environ Technol Innov 26:102336.

Youssef FS, Ismail SH, Fouad OA, *et al.,* 2024. Green synthesis and biomedical applications of zinc oxide nanoparticles. Review. Egypt J Vet Sci 55:287-311.

Zahra M, Chota A, Abrahamse H, *et al.,* 2023. Efficacy of green synthesized nanoparticles in photodynamic therapy: A therapeutic approach. Int J Mol Sci 24:10931.